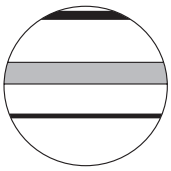

Research Paper

The Holocene
2021, Vol. 31(7) 1124–1137

DOI: 10.1177/09596836211003214
journals.sagepub.com/home/hol

Late-Holocene diatom community response to climate driven chemical changes in a small, subarctic lake, Northwest Territories, Canada

Paul B Hamilton,[1] Scott J Hutchinson,[2] R Timothy Patterson,[2] Jennifer M Galloway,[3,4] Nawaf A Nasser,[2] Christopher Spence,[5] Mike J Palmer[6] and Hendrik Falck[7]

Abstract

The paleolimnological record of diatoms and climate, spanning the last 2800 years, was investigated in a small subarctic lake (Pocket Lake) that from AD 1948 to 2004 was contaminated by gold smelting waste. An age-depth model was constructed using a combination of ^{210}Pb, ^{14}C, and tephra to determine a 2800 year history of lake ontogeny (natural aging), biological diversity, and regional climate variability. Diatoms form six strong paleoecological assemblages over time in response to changes in local hydrological and sedimentological conditions (including metals). Selected environmental variables explained 28.8% of the variance in the diatom assemblages, with Fe, Ca, and sediment end member distribution being important indicators. The diatom assemblages correlated to the Iron Age Cold Epoch (2800–2300 cal BP), Roman Warm Period (2250–1610 cal BP), Dark Age Cold Period (1500–1050 cal BP), Medieval Climate Anomaly (ca. 1100–800 cal BP), and the Little Ice Age (800–200 cal BP). The disappearance of *Staurosira venter* highlights the change from the Iron Age Cold Epoch to the Roman Warm Period. After deposition of the White River Ash (833–850 CE; 1117–1100 cal BP), transition to circumneutral conditions was followed in tandem by a transition to planktic influenced communities. Ten discrete peaks of Cu, Pb, and Zn were observed and attributed to soluble mobility from catchment soils through enhanced seepage and spring snowmelt. The prominent metal spikes were aligned with increases in *Brachysira neoexilis*. Downward mobilization of arsenic and antimony from contaminated surficial sediments highlight the problem of post depositional industrial contamination of paleosediments. Results demonstrate that paleoclimatic changes in the region, modulated by solar radiation, impacted temperature and precipitation in the lake catchment, influencing temporal shifts in diatom ecology. Changes in diatom taxa richness provided valuable information on the relative influence of water quality (planktic taxa) and sediment input (benthic taxa). The diatom assemblage succession also provides evidence that natural aging over time has played a role in the ecological evolution of the lake.

Keywords

alkalinity, assemblage dynamics, diatoms, Late-Holocene, metals, Northwest Territories, pH, regional climate

Received 22 January 2021; revised manuscript accepted 8 February 2021

Introduction

High northern latitudes have been disproportionately affected by 21st century climate change relative to other regions (ACIA, 2004; Callaghan et al., 2013; Delworth et al., 2016). Both freshwater and marine ecosystems in the Arctic have changed with exponential-like increases in freshwater productivity, biomass, and the introduction of southern species (e.g. Prowse et al. 2006; Vincent, 2020). In addition, legacy contamination from resource development, can amplify impacts related to environmental and anthropogenic stressors (e.g. Galloway et al., 2018; Hamilton et al., 2015; Nasser et al., 2016; Thienpont et al., 2016). Paleolimnological records offer a means to establish pre-development (including mining) chemical and biological background conditions that can be used to clarify environmental assessments and predict ecosystem responses to ongoing and future environmental change (MacDonald et al., 2005). For example, Late-Holocene climatic variation has been documented from lake sediment records in northwestern Canada (e.g. Bennike et al., 2004; Pienitz et al., 1999; Sulphur et al., 2016; Upiter et al., 2014; Viau and Gajewski, 2009; Wolfe et al., 1996). These studies examined changes in biota (diatoms, pollen, chironomid head-capsules) and grain size to determine lacustrine environmental conditions, including biogeographical setting, regional climate, and conditions of the catchment. Diatoms as a proxy, are robust

[1]Collections and Research Division, Canadian Museum of Nature, Canada
[2]Ottawa-Carleton Geoscience Center and Department of Earth Sciences, Carleton University, Canada
[3]Aarhus Institute of Advanced Studies, Aarhus University, Denmark
[4]Geological Survey of Canada, Natural Resources Canada, Canada
[5]Environment and Climate Change Canada, Canada
[6]North Slave Research Centre, Aurora Research Institute, Aurora College, Canada
[7]Northwest Territories Geological Survey, Canada

Corresponding author:
Paul B Hamilton, Research Division, Canadian Museum of Nature, P.O. Box 3443, Ottawa, ON K1P 6P4, Canada.
Email: phamilton@nature.ca

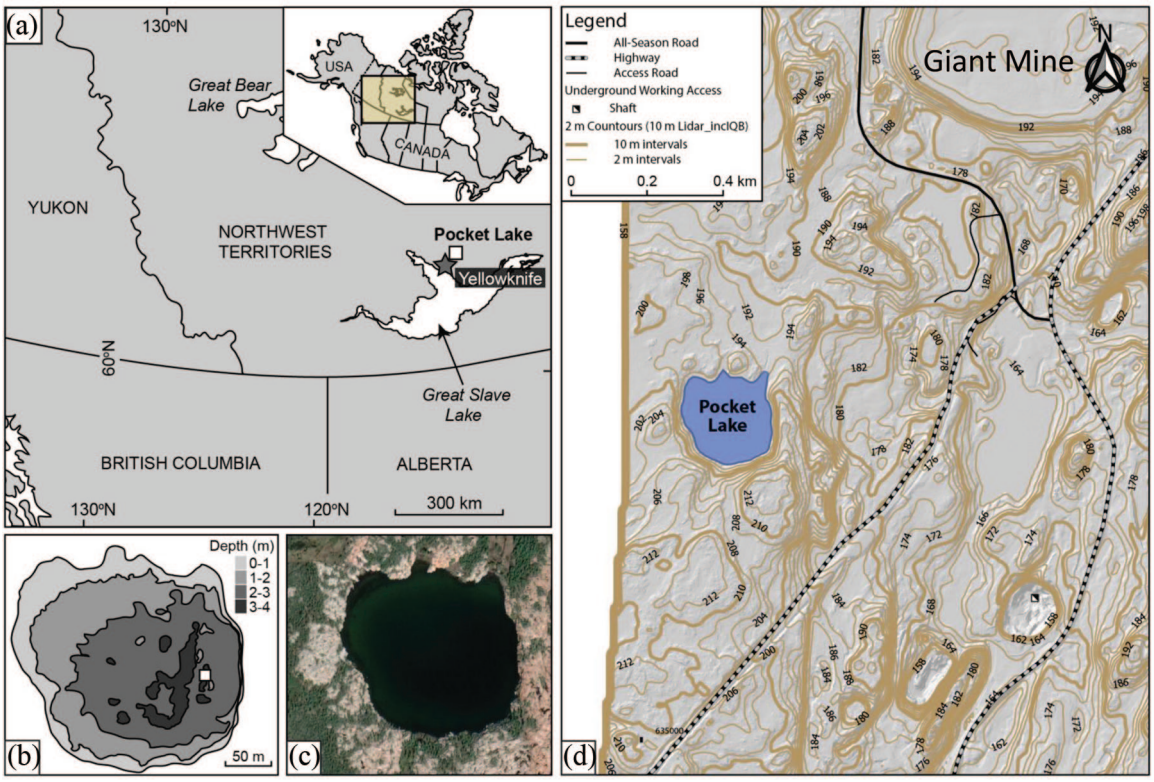

Figure 1. Location of Pocket Lake within the Northwest Territories, Canada: (a) geographic map of Canada (right insert) and the lake location, north of Great Slave Lake, (b) bathymetry of Pocket Lake (m), (c) Pocket Lake (dark green-black) with immediate basin area (trees: green; grey-pink: bedrock), and (d) Lidar contours of the area around Pocket Lake (2 and 10 m meter intervals are presented).

indicators of changes in lake systems because taxa are widespread, numerous, and sensitive to environmental parameters, such as surface water pH, alkalinity, and nutrient concentrations (Smol and Stoermer, 2010).

This study assessed changes in diatom community composition between ~2850 and 200 cal BP as recorded in the sedimentary record of Pocket Lake, a small, subarctic lake in the central Northwest Territories, Canada, near the city of Yellowknife and on the property of the former Giant Mine (operation: 1948–1999). The study period predates the impact of local anthropogenic mining activities (Jamieson, 2014). Diatom assemblages were identified and compared with lake growth conditions (benthic, planktic systems), sediment chemistry, and particle size data from freeze-cores, and with a previous reconstruction of total solar irradiance (TSI; Steinhilber et al., 2009). This multi-proxy approach was used to explore diatom community responses to variations in chemical parameters and the role of solar radiation as a lake ecosystem modulator (e.g. Dalton et al., 2018; Gregory et al., 2021). Through the synthesis of these datasets, late-Holocene changes in the water and sediment structure of Pocket Lake over the past almost three millennia were reconstructed. This is relevant because Pocket Lake is currently contaminated by emissions from the Giant Mine with near-surface sediments containing arsenic (As) concentrations over 30,000 mg kg^{-1} (Thienpont et al., 2016). At this site, as well as other contaminated lakes in the region (see Galloway et al., 2018), it is critical to have information on the response of lake biota to natural, pre-industrial chemical change. This information will help strategically form environmental management practices at contaminated sites where element mobility may be influenced by 21st c. warming (Miller et al., 2010). Previous work at Pocket Lake also identified this site as ideal due the establishment of a robust sedimentary chronology that facilitates the present study (Patterson et al., 2017).

Study site

Pocket Lake (114.3719 W, 62.5090 N) is a headwater subarctic lake with a small catchment (<5 ha) located adjacent to the Giant Mine site roughly 4 km north of Yellowknife, Northwest Territories, Canada (Figure 1). Pocket Lake is situated within the southern portion of the Baker Creek watershed, which drains into Yellowknife Bay and Great Slave Lake. The lake is close (<1 km) to the Giant Gold Mine roaster. The paleo-sediment record presented here from Pocket Lake, as determined by ^{210}Pb dating, terminates at ~200 cal BP (13 cm) well before the onset of large-scale mining in the region. The recent anthropogenic impact of mining was not investigated since this part of the record has been previously analyzed, revealing substantial levels of contamination by mining associated metal(loid)s, including As and Sb (Thienpont et al., 2016). The catchment for Pocket Lake is dominated by exposed bedrock outcrops (78% cover). A large soil filled valley (22% catchment cover) drains from the north side of the lake and has been the site of extensive hydrological investigation since the 1970s (Spence and Woo, 2003) (Figure 1). LiDAR results show the lake is surrounded by a low-relief catchment (<20 m). The vegetation is predominately in the soil valley with marginal Black spruce (*Picea mariana*), scattered willows (*Salix* spp.), and ground cover of mosses, sedges, and grasses. At the time of sampling the lake was oligotrophic, with a pH and conductance of 7.7 and 494 µs cm^{-1} respectively. The average annual temperature between 1942 and 2007 was −4.8 ± 1.4°C, rainfall 155 ± 47 (mm), and snow 138 ± 45 cm (Environment Canada, Yellowknife Airport Station). Ice (<1 m thick) covers the lake for ca. 7 months each year. Hydrological inputs to the lake are primarily through annual snowmelt runoff, and to a lesser degree through sporadic rainfall events (Spence and Woo, 2003).

Pocket Lake is located within the Slave Geologic Province. The bedrock underlying the catchment is composed of Archean granodiorite belonging to the Defeat Plutonic Suite (Henderson,

1985). The southernmost of a pair of ENE trending 2.19 Ma Dogrib diabase dykes intrudes the granodiorite approximately 30 m north of the Pocket Lake basin. The southern dyke has a width of 40–45 m and is one of the widest dykes in the region. The dyke is composed of partly saussuritized plagioclase laths poikilitically enclosed in zoned clinopyroxene crystals with trace ilmenite in titanomagnetite. The quartz–alkali feldspar-rich laths contain minor Fe-rich biotite, chlorite, epidote, and trace amounts of apatite, allanite, ilmenite, chalcopyrite, sphalerite, baddeleyite, zirconolite, and zircon (Henderson, 1985).

The Pocket lake basin is also located 100 m west of the West Bay Fault, a Proterozoic fault that separates the intrusive rocks from the Yellowknife Supercrustal rocks that host gold deposits and the lake. The West Bay Fault is approximately 250 km in length and has an average horizontal displacement of 5 km (Brown, 1955; Henderson, 1985). Quartz-cemented breccia and multiple generations of cross-cutting quartz veins in the fault zone indicate a complex history of fault and fluid movement (Ripple, 2007 Per. Comm.). The Yellowknife Supergroup is composed of mafic meta-volcanic rocks interbedded with meta-sedimentary and felsic volcaniclastic horizons (Boyle, 1960; Henderson, 1985). The volcanic belt forms the western margin of a basin filled by meta-sedimentary rocks consisting of greywacke, slate, schist, and phyllite. The volcanic belt is primarily comprised of basalt, andesite, and pillowed flows which form a homoclinal north-south belt (Boyle, 1960).

Methodology

Field work

Two cores, PKT_2FR and PKT_1FR, were collected approximately 3 m apart from Pocket Lake in 2012 using a custom designed freeze corer (Patterson and Kumar, 2002). Reference to individual faces on each core are designated by F1 and F2 suffixes where applicable (e.g. PKT_2FR_F1; PKT_2FR_F2). The cores were collected from a water depth of ~3.5 m near the deepest part of the lake (Z_{max}). Freeze-cores are ideal for the collection of sedimentary records in low sedimentation environments and allow for extremely high-resolution sub-sampling (Macumber et al., 2011). Freeze core PKT_2FR was 131 cm in length while core PKT_1FR was 180 cm long. Core PKT_1FR did not capture the sediment-water interface due to over penetration during core collection. Therefore, this diatom study focuses on sediments in core PKT_2FR_F2. The cores were subsampled at mm-resolution using a custom designed sledge microtome (Macumber et al., 2011). The primary samples were from 13 to 131 cm in PKT_2FR_F2. One-mm thick sub-samples at 1-cm intervals were used for diatom ($n=118$), and sediment chemical analysis ($n=118$), while the remaining 1-mm sub-samples were used for particle size analysis ($n=913$). Rock-Eval pyrolysis ($n=85$) was conducted on sediments collected in core PKT_1FR at 1-cm intervals (note, some intervals had minimal organic sample volumes).

Diatom analysis

Sediment sub-samples were prepared for diatom analysis following a modified version of the protocol outlined in Gajewski et al. (1997). Samples of 10 mg aliquots were placed in centrifuge tubes and freeze dried. Sub-samples of specific weight were then placed in individual beakers and 10 ml of 1:1 concentrated sulfuric (H_2SO_4) and nitric (HNO_3) acid solution were added and heated to digest organic material. The remaining residues were diluted to neutrality and 0.8 ml were placed using volumetric pipettes onto clear cover glasses and left to dry for 24 h. The cover glasses were mounted to glass slides using Naphrax®, a permanent adhesive with a high refractive index (1.65). Diatom counts were carried out at contiguous 1-cm intervals throughout the PKT_2FR_F2 core using an Olympus BX51 light microscope with a 100× oil immersion objective (splan, 1.25). A minimum of 200–600 valves were counted in each preparation and identified to the lowest possible taxonomic level with reference to photomicrographs of taxa from similar geographic regions and environments (Antoniades et al., 2008; Bahls et al., 2018; Krammer and Lange-Bertalot, 1985–1991). Current taxonomic classifications follow Guiry and Guiry (2020).

Chronology

Two cores (PKT_1FR; PKT_2FR) were used in this study. The age-depth relationship for both cores was published in Patterson et al. (2017) and is based on the presence of the White River Ash (WRAe; 833–850 CE; 1117–1100 cal BP) in both cores as well as 10 AMS ^{14}C determinations on bulk sediment at the A.E. Lalonde AMS Laboratory in Ottawa, Ontario and the 14CHRONO Dating Laboratory in Belfast, Northern Ireland (Table 1). Bulk sediment was used for dating because macrofossils were absent. Analysis pretreatment details are provided in Patterson et al. (2017). Radiocarbon dates were calibrated with OxCal v4.2 (Bronk Ramsey, 2009) using the IntCal13 calibration curve (Reimer et al., 2013). The Bacon 2.2 computer program (Blaauw and Chisten, 2011, 2013) was then used to develop the final age-depth model for the core using the occurrence and known age of the WRAe (ca. 0.5 cm) preserved in the Pocket Lake core and accumulation rate and memory parameter values for lakes within the central Northwest Territories (Crann et al., 2015; Figure 2). The sediment accumulation rate (SAR) was calculated by dividing each 1-cm interval by the approximate time interval indicated by the age-depth model. Core PKT_1FR collected ~3 m away from the primary core was aligned to the primary core by additional 11 AMS ^{14}C dates on PKT_1FR with alignments on tephra and sediment wedge anchor points.

Element geochemistry

Sub-samples were freeze dried and screened to <180 µm (−80 mesh ASTM) in the laboratory. Concentrations of elements were determined by inductively coupled plasma-mass spectrometry (ICP-MS) (ICP-MS 1F/AQ250 package) following digestion by a modified *aqua regia* treatment (0.50 g of sample digested in a solution of 2.0 mL HCl, 2.0 mL HNO_3, and 2.0 mL H_2O at 95°C for 1 h) with the exception of phosphorus, which was extracted using $NaHCO_3$. In total, 45 elements were analyzed at 1 cm intervals through the core ($n=5445$). Partial digestion with *aqua regia* was used to extract metal(loid)s because complete digestion methods that involve high-temperature fuming can volatilize elements like As and Sb, both contaminants of potential concern in this study (Parsons et al., 2012; Ritchie et al., 2013). Analyses were conducted at Acme Laboratories, Vancouver, Canada, job number VAN14000607 for core section PKT_2FRF1. The validation of the element analyses and the reproducibility of the results is presented in Supplemental S1.

Rock-Eval pyrolysis and total solar irradiance

Rock-Eval® 6 pyrolysis was used to analyze organic constituents of the sediments (Vinci Technologies, Rueil-Malmaison, France; Lafargue et al., 1998). Pyrolysis was only carried out on 85 sub-samples from the PKT_1FR core due to insufficient organic material remaining from either face of PKT_2FR. Direct comparison between the cores was possible based on the detailed age model developed by Patterson et al. (2017; Figure 2) for PKT_2FR, with AMs dates from PKT_1FR and two anchor-point layers (1: Tephra [WRAe (55.5 cm)], 2: sand/mud spike near the bottom of the core (120 cm)). The Rock-Eval® 6 instrument processes organic matter under an inert (N_2) atmosphere and oxidizes organic matter by programed temperature heating of bulk

Table 1. Radiocarbon dates from the two Pocket Lake cores, calibrated with the IntCal13 calibration curve (Reimer et al., 2013) using OxCal v4.2.4 (Bronk Ramsey, 2009) following the conventions of Millard (2014). Data derived from Patterson et al. (2017).

	Lab ID	Depth (cm)	^{14}C age BP	Pretreatment	Cal BP
PKT_2FRF1	UBA-20676	10–10.5	362 ± 27	Acid only	500–422 (50.7%)
					400–316(44.7%)
	UBA-22350	20–20.5	731 ± 31	Acid only	727–653 (95.4%)
	UBA-20679	52–52.5	1335 ± 25	Acid only	1302–1339 (85.5%)
					1205–1186 (9.9%)
	Tephra	55–56			1110 ± 50
	UBA-22351	57–57.5	1394 ± 30	Acid only	1350–1279 (95.4%)
	UBA-22352	70–70.5	1725 ± 31	Acid only	1707–1561 (95.4%)
	UBA-20678	128.5–129	2966 ± 26	Acid only	3215–3057 (93.9%)
					3049–3035(1.3%)
PKT_1F	UBA-20680	35.5–36	795 ± 27	Acid only	674–759 (95.4%)
	Tephra	35–36			1110 ± 50
	UBA-22346	56–56.5	1401 ± 27	Acid only	1349–1385 (95.4%)
	UOC-653	60–60.5	1607 ± 29	Acid only	1555–1413 (95.4%)
	UOC-654	60–60.5	1553 ± 27	AAA	1526–1386 (95.4%)
	UBA-22347	83.5–84	2145 ± 31	Acid only	2304–2238 (24.9%)
					2182–2037 (68.2%)
					2025–2007 (2.4%)
	UOC-655	109–109.5	2918 ± 26	Acid only	3158–2970 (95.4%)
	UOC-656	109–109.5	2960 ± 27	AAA	3211–3007 (95.4%)
	UOC-733	109–109.5	3029 ± 19	AAA	3334–3290 (20.9%)
					3257–3166(74.5%)
	UOC-734	109–109.5	3088 ± 19	AAA	3363–3241 (95.4%)
	UOC-923	140–140.5	3739 ± 27	Acid only	4321–4308 (2.0%)
					4156–4061 (62.8%)
					4052–3986 (30.7%)
	UOC-924	180–180.5	4254 ± 31	Acid only	4868–4813 (83.1%)

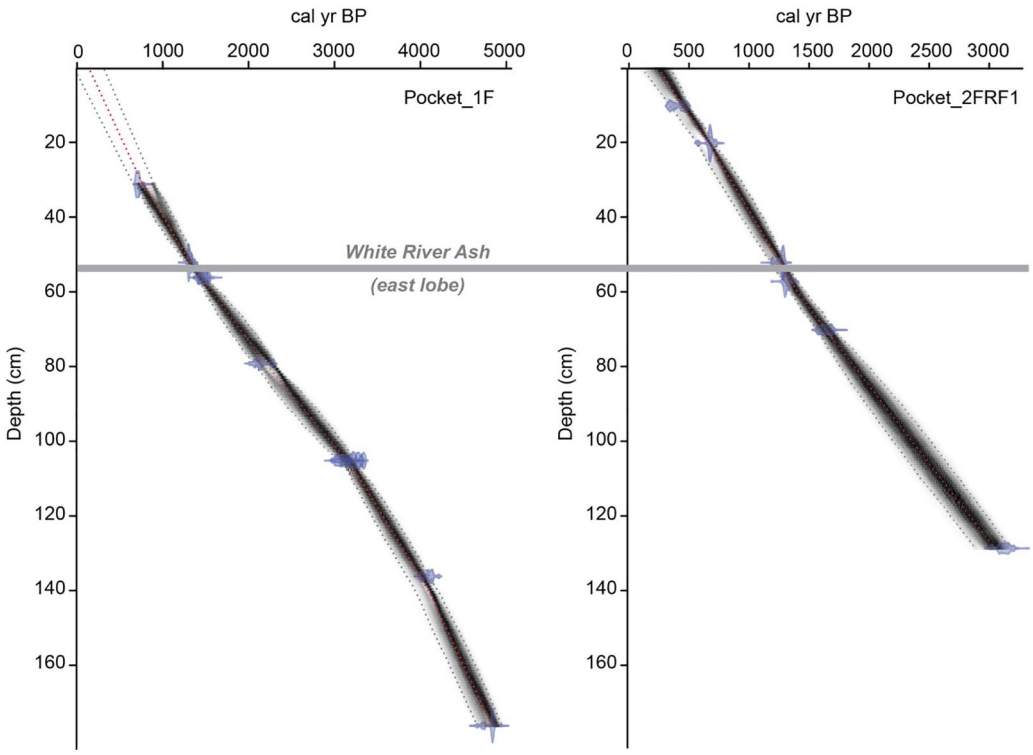

Figure 2. Age-depth models for Pocket Lake freeze cores PKT_1FR and PKT_2FRF1 showing the depth of the White River Ash (1110 ± 50 cal BP) marker bed, and analyzed radiocarbon dates. Models were created using Bacon v2.2 (Blaauw and Christen, 2011) and the IntCal13 calibration curve (Reimer et al., 2013). Figure modified after Patterson et al. (2017).

sediments (~20 mg; heating rate of 25°C min^{-1}). Rock-Eval® 6 pyrolysis measures the quantity of labile, readily degradable hydrocarbon devolatilized at 300°C (S1, mg hydrocarbon g^{-1}), the hydrogen-rich, higher molecular weight kerogen-derived hydrocarbon released by thermal cracking of organic matter at 650°C (S2, mg hydrocarbon g^{-1}), the amount of carbon dioxide

released during pyrolysis of kerogen (S3, mg hydrocarbon g^{-1}), and refractory, residual carbon (RC wt. %) measured by automated transferal to an oxidation oven and heated from 400°C to 850°C. Total Organic Carbon (TOC; wt. %) represents the quantity of all organic matter released during pyrolysis and oxidation heating. S1, S2, and S3 were converted to wt. % by multiplying by 0.083 (Sanei and Goodarzi, 2006). Analyses of standard reference materials (IFP 160000, Institut Français du Pétrole and internal 9107 shale standard, Geological Survey of Canada, Calgary; Ardakani et al., 2016) was run for every fifth sample and showed accuracy and precision to be better than 5% relative standard deviation. Due to low sample volumes, absolute values cannot be used, but trends can be followed and analyzed. S2 compounds are typically derived from the highly aliphatic biomacromolecule structure of algal cell walls and other aquatic biological matter and are used in this study to evaluate autochthonous biomass (Carrie et al., 2012; Sanei et al., 2005). Total solar irradiance data was extracted from another regional study close to Pocket Lake (Steinhilber et al. 2009). The data from Steinhilber et al. (2009) were lined up with sample dates from this study and TSI values extracted.

Particle size analysis

Sedimentary particle size was determined at consecutive 1-mm intervals from 13 to 131 cm depth ($n = 913$) in core PKT_2FR_F2. Analyses were conducted using a Beckman Coulter LS 13 320 laser diffraction particle size analyzer fitted with a universal liquid module and a measurement range between 0.37 and 2000 µm. Hydrogen peroxide (30%) was added to sub-samples in an 80°C water bath to oxidize organic matter prior to analysis (Murray, 2002; Van Hengstum et al., 2007). The samples were loaded into the instrument until an obscuration level of $10 \pm 3\%$ was attained. Summary statistics were compiled using GRADISTAT (Version 8; Blott and Pye, 2001). Two reference materials were used: an accuracy standard provided by Beckman Coulter (Garnet15: mean diameter 15 µm) run once per month and an in-house mud sample (inhouse Cushendun Mud standard) as a precision control analyzed at the beginning of every session.

End-member mixing analysis (EMMA) was performed on the resulting particle size dataset to characterize depositional processes influencing sedimentation in the lake. Lacustrine sediments typically have polymodal particle size distributions, which is attributed to the mixing of unimodal particles from various sources (i.e. sediment reworking). EMMA results can untangle complex polymodal particle size distributions that can be linked to specific sedimentary processes and to comminution properties of local bedrock. EMMA was carried out following the procedure outlined in Dietze et al. (2012, 2014) using the R package, EMMAgeo (version: 0.9.7, Dietze and Dietze, 2016). Only robust end members, those recurring in the majority of model runs and not overlapping, were included in subsequent analyses (after Macumber et al., 2018).

Statistical analyses

All statistical analyses employed in this study were conducted in the R environment (version 4.0.0) (R Core Team, 2020). Counts of diatom taxa from each sample were converted to relative abundances for subsequent assessment of changes in assemblage structure. Only taxa present in significant numbers in at least one sample throughout the core were included in the subsequent analysis. Taxa to be included in statistical analyses were determined using a technique outlined in Fishbein and Patterson (1993) whereby standard errors were calculated for individual taxon in each sub-sample. A taxon was deemed to be present in statistically significant numbers if the relative abundance exceeded the standard error. A total of 114 diatom taxa were initially identified, of which 65 species were present in statistically significant quantity and included in subsequent statistical analyses (see Supplemental S7 for taxa studied). Relative abundances of the statistically significant taxa were Hellinger transformed and ordinated using Non-metric Multidimensional Scaling (NMDS) to group samples with similar diatom assemblage composition. NMDS ordination was used because this approach does not assume any environmental gradient relationship (Paliy and Shankar, 2016).

Stratigraphically Constrained Incremental Sum of Squares (CONISS; Grimm, 1987) cluster analysis was conducted on the Hellinger transformed dataset of statistically significant diatom taxa using the rioja package in RStudio with Ward's minimum variance method and Euclidean distances to identify stratigraphic zones based on changes in diatom community composition. Assemblage stratigraphic zones were visually identified using the results from CONISS and NMDS. Redundancy analysis (RDA) was used to evaluate relationships between diatom assemblages and environmental variables. Partial RDA analysis with a permutation test was performed on the selected variables to determine the percent of variance in the diatom distribution explained by each variable. The environmental variables examined or used in the final RDA model were selected to maximize the variance explained while maintaining the fewest number of significant variables. The variables were determined using an iterative approach whereby the available parameters were incrementally added to the model and eliminated if they did not explain more than ~2% of variance. TSI, with a low explained variance, was retained as it is known to provide an independent signal of climate. The final variables identified as potential ecosystem drivers were those that did not co-vary with any other variables in the model. A Spearman Rank Correlation was performed on the environmental data set to identify correlated variables (Supplemental S2). Variables with a $r_s > 0.6$ ($p < 0.05$) were deemed to be strongly correlated. S2 productivity from the companion core was included in this analysis to evaluate trends in productivity, but these data should be interpreted with caution due to small sample sizes.

Results

Sediment accumulation rate (SAR)

The SAR varied throughout the core ranging from 0.3 to 0.6 mm $year^{-1}$ (Figure 3). In the basal portion of core PKT_2FR_F2 (131–115 cm; ca. 2890–2460 cal BP), the SAR averaged 0.4 mm $year^{-1}$. From 114 to 101 cm (2460–2220 cal BP) the SAR rose to 0.6 mm $year^{-1}$. In the 100–63 cm (ca. 2200–1280 cal BP) interval the SAR again fell to 0.4 mm $year^{-1}$ before increasing to 0.5 mm $year^{-1}$ from 55 to 25 cm (ca. 1110–500 cal BP). In the uppermost portion of the core examined (25–14 cm; 500–200 cal BP) the SAR was 0.3 mm $year^{-1}$.

End-member mixing analysis (EMMA)

Four end-members were identified using EMMA (Figure 3). End-member 1 (EM1; 1.3 µm), was found above 97 cm (ca. 2150 cal BP) in the PKT_2FR-F2 core and was prominent in the 13 cm (ca. 200 cal BP) to 19 cm (ca. 350 cal BP) interval, with increases lower in the core at 35 (ca. 700 cal BP) and 52 cm (ca. 1050 cal BP). End-member 2 (EM2; 5.6 µm) was found in highly variable proportions through the core, and was particularly low below the 97 cm (ca. 2150 cal BP) and above the 15 cm (<250 cal BP) horizons. End-member 3 (EM3; 15.7 µm) was found throughout the core, and as with EM2, was highly variable in its occurrence. It generally increased in abundance downcore (57–120 cm; ca. 1150–2610 cal BP). End-member 4 (EM4; 36.2 µm) was present in notable levels across four intervals of the core: 13–15 cm (ca.

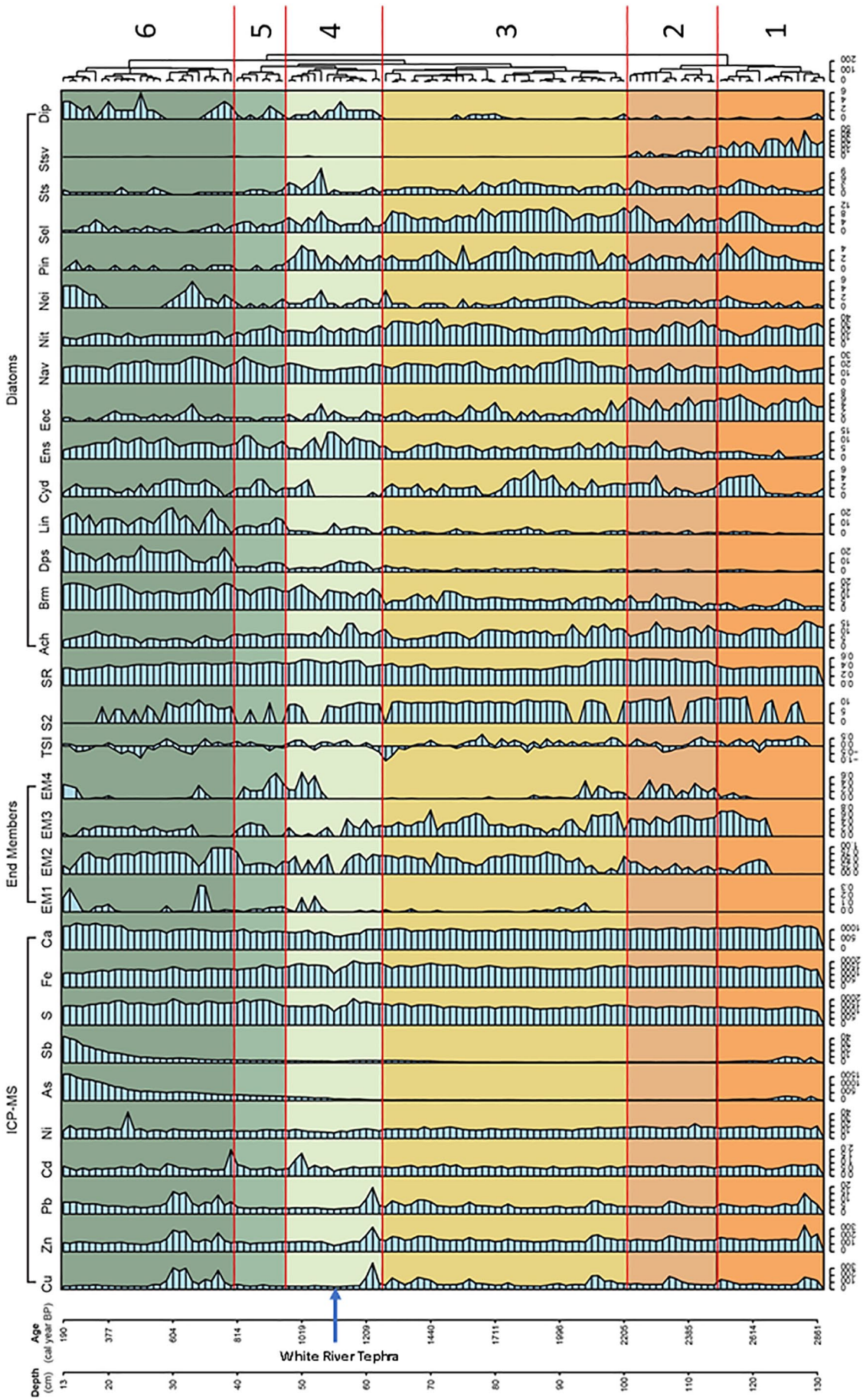

Figure 3. Stratigraphic profiles of significant diatoms and environmental parameters determined by iterative redundancy analysis (RDA) for core PKT_2FR_F2. Core depth (cm) and cal BP are presented on the left axis and CONISS diatom assemblage groups are on the right. The graphs comprise sedimentary metal and metaloids (mg kg^{-1}), particle size end-members (relative abundance; EM1: 1.3 µm; EM2: 5.6 µm; EM3: 15.7 µm; EM4: 36.2 µm), TSI (Wm^{-2}), productivity S2 (wt. %), sedimentation rate (mm yr^{-1}) and diatom taxa (% abundance) preserved in the sediment profile of Pocket Lake. S2 values were obtained from core PKT_1FR1 and were related to the PKT_2FR1 datasets based on the age model for PKT_1FR1 and the stratigraphic occurrence of the White River Ash.
Ach: *Achnanthidium* spp.; Brm: *Brachysira neoexilis*; Cyd: *Cyclotella* spp.; Dps: *Discotella pseudostelligera*; Eec: *Encyonema* spp; Ens: *Encyonopsis* spp; Lin: *Lindavia intermedia*; Nit: *Nitzschia* spp.; Nas: *Navicula* spp.; Nei: *Neidium* spp.; Pin: *Pinnularia* spp.; Sel: *Sellaphora* spp.; Sts: *Staurosira venter*.

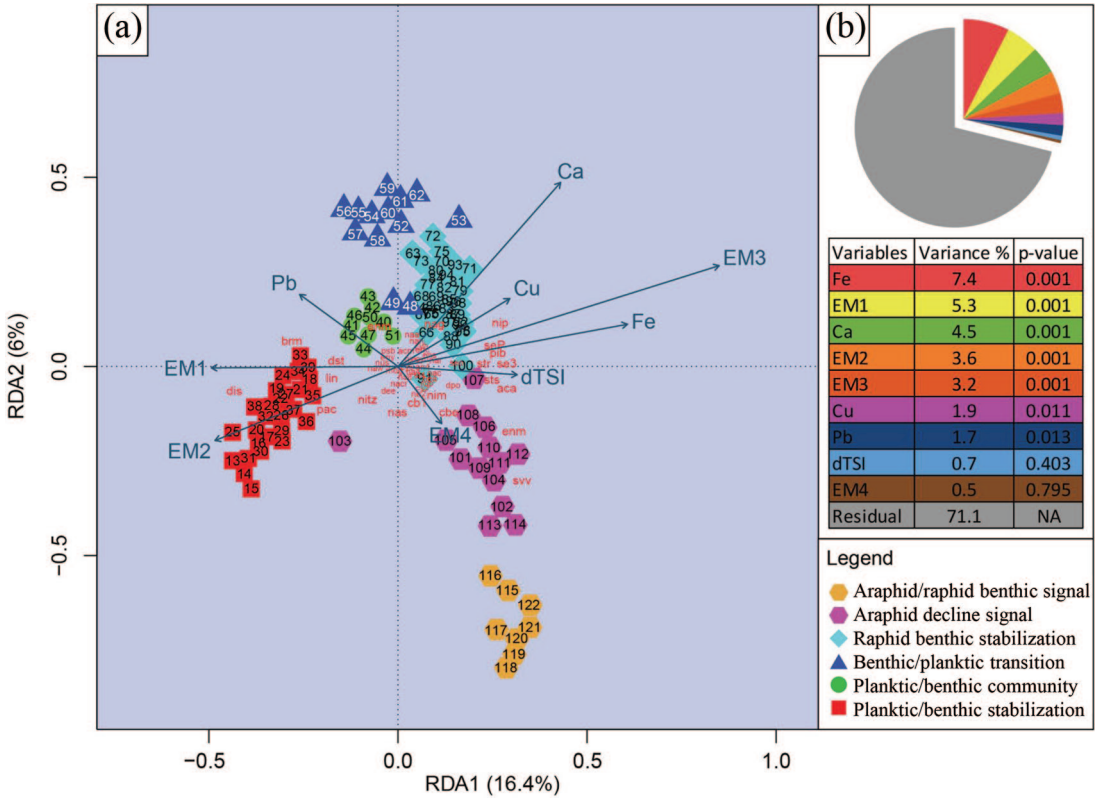

Figure 4. RDA tri-plot.
Each point represents an individual sample with the numerical value denoting sample depth. Color groups were based on cluster analysis (CONISS) of species data. Orange = Assemblage 1 (2850–2460 cal BP); Purple = Assemblage 2 (2460–2210 cal BP); Turquoise = Assemblage 3 (2210–1270 cal BP); Dark Blue = Assemblage 4 (1270–980 cal BP); Green = Assemblage 5 (980–800 cal BP); Red = Assemblage 6 (800–200 cal BP). The line projections represent different environmental parameters included in the model. The length of the line relates to the variance explained by the parameter. Taxa are plotted in red as text; codes with taxa identifications are found in Supplemental S7. Ca = Calcium; Cu = Copper; Fe = Iron; Pb = Lead; EM:1.3 µm; EM2: 5.6 µm; EM3: 15.7 µm; EM4: 36.2 µm. TSI = Total solar Irradiance (after Steinhilber et al., 2009). The pie chart indicates the variance explained as a percentage for each variable included in the model as well as the residual variance. The table provides their numerical values for variance explained and associated *p*-values.

200–250 cal BP); 33.5 cm (ca. 675 cal BP); 42–52 cm (ca. 850–1050 cal BP), and; 85–121.5 cm (ca. 1850–2640 cal BP). Higher proportions of EM4 were aligned with increasing EM1.

Rock-Eval pyrolysis

The S2 values ranged between 6.3 and 13.4 wt. % with a median of 10.5 wt. % in the sediment sections (Figure 3). Low sample concentrations with potential high variability limit the quantitative integrity of the results. However, trends and presence/absence indicators are valid. There was a general increasing trend in productivity downcore from 20 to 128 cm (377–2800 cal BP). Thorough the periods 131–101 cm (ca. 2890–2220 cal BP) and 100–63 cm (ca. 2250–1280 cal BP) there were consistent levels of production. The interval 62–48 cm (ca. 1280–980 cal BP) showed a slight declining trend in productivity, while during the Medieval Warm Anomaly (MWA) (47–40 cm; ca. 960–810 cal BP) there was a decline in productivity. More recently, through the Little Ice Age (LIA; Mann et al., 2009) (800–200 cal BP), S2 had consistent values to 580 cal BP, then trending declines through to 200 cal BP.

Bulk sediment chemistry

Sediment chemistry varied throughout core PKT_2FR_F1 and some patterns of concomitant changes were observed between elements. Copper, Zn, and Pb were positively correlated through the sediment record, and three large increases (1233, 751, and 647 cal BP) and seven smaller increases from 1250 to 2800 cal BP were observed (Figure 3). Iron, S, and Ca were correlated from 2800 cal BP to the mid-interval of the MWA (ca. 900 cal BP). Iron was the most prominent metal from the bottom of the core to 37 cm (2800–750 cal BP), then S increased and became the dominant metal to 20 cm (750–200 cal BP). Calcium levels were consistent through the core until an increase occurred at the top from 22 to 13 cm (425–200 cal BP). The highest concentrations of As (1500 mg kg^{-1}) and Sb (40 mg kg^{-1}) in the sedimentary record were measured in the upper most sediment of the core (13 cm; 200 cal BP) and declined to ca. 55 cm (1110 cal BP), where concentrations of As and Sb were 107 and 1.6 mg kg^{-1}, respectively. Throughout the core, As and Sb were positively correlated (rho = 0.91, $p = 0.001$; $n = 118$). Below the WRAe tephra layer (55.5 cm), As and Sb were present in lower concentrations (<110 mg kg^{-1}) except near the bottom of the core (129–123 cm; 2840–2690 cal BP) where concentrations were elevated relative to concentrations in the bottom half of the core and reached 278 mg kg^{-1} As and 10 mg kg^{-1} Sb. Cadmium was measured in low concentrations (<1 mg kg^{-1}) through most of the core except for two peaks (795 and 1029 cal BP), which were not associated with increases in other metals. There was little variation in Ni concentrations through the sedimentary record except for one peak (43 mg kg^{-1}) at approximately 25 cm (500 cal BP), which was coincident with the increase in Ca towards more recent time. In the WRAe (55.5 cm, 1110 cal BP) all metals (excluding Si) were at the lowest levels throughout the 2800 years.

Diatom analysis

The majority of the observed diatom species preserved in the ~2850–200 cal BP PKT_2FR_F2 core were benthic taxa from the genera *Achnanthidium*, *Brachysira*, *Navicula*, *Nitzschia*, *Sellaphora*,

and *Staurosira* (Supplemental S3 and S4). Taxa from other genera of interest included *Encyonema*, *Encyonopsis*, *Neidium*, *Nupela*, *Pinnularia*, and *Stauroneis* (Supplemental S3). Planktic species were composed of the genera *Cyclotella*, *Lindavia*, *Discotella*, and *Pantocekiella* (Supplemental S5). The metal tolerant species *Aulacoseira pseudomuzanensis* was present, but rare (Supplemental S5). The abundance of planktic diatoms was higher in the younger, relative to older sediments of the core, but never made up more than ~25% of the total diatom assemblage (Figure 3).

Six diatom assemblages were identified using CONISS and NMDS analyses (Figures 3 and 4 and Supplemental S6). One sample (103) from Assemblage 2 was not aligned with other members of Assemblage 2 with CONISS, while samples 91 (assemblage 3), 48, 59, 53 (assemblage 4) were outliers under MSDS (Figure 4, Supplemental S6). The less abundant diatom taxa in these assemblages consistently exhibited the greatest stratigraphic variation, whereas the dominant taxa within the genera *Nitzschia* spp. and *Navicula* spp., maintained relatively stable abundances (Figure 3).

Assemblage 1: Araphid/raphid benthic signal (131–115 cm; ca. 2850–2460 cal BP, n = *17)*

Nitzschia spp. (dominant taxon *N. alpina sensu lato*) was the most common genus in the basal sediments of core (PKT_2FR_F2) (zonal median relative abundance of 25%; range: 13%–34%) (Figure 3). *Navicula* spp. also made up a large proportion of the diatom population with a median abundance of 17% (13%–22%). *Navicula cryptocephala* was the dominant single species of this genus ranging from 2.5% to 11%. Another significant constituent of Assemblage 1 was *Staurosira venter* (median: 18.4%; range: 3%–50%). Less common taxa in this interval included *Achnanthidium* spp., *Sellaphora pupula* s.l., *Brachysira neoexilis*, and *Encyonema minutum* (ranges between 1% and 18%). The biotic structure of Assemblage 1 changed through this interval. *Staurosira venter* decreased from a maximum of 50% at ca. 2810 cal BP (128 cm) to a minimum of 3% at ca. 2640 cal BP (121 cm). Conversely, *Pinnularia biceps* and *Sellaphora* spp. increased from 1% to 5% and 3% to 10%, respectively. The planktic taxon *Cyclotella* spp. (including *C. distinguenda*) appeared (5%) then disappeared towards the end of this interval. Other planktic taxa including, *Lindavia intermedia*, *Pantocekiella comensis*, and *Discotella pseudostelligera* (including *D. lacuskarluki*) were present in low numbers with a planktic:benthic ratio <0.04.

Assemblage 2: Araphid decline signal (114–101 cm; ca. 2460–2210 cal BP, n = *15)*

Nitzschia alpina was dominant through this assemblage (median: 28.6; range: 19%–38%), with a weak decline from 2300 to 2210 cal BP (Figure 3). *Navicula* spp. (median: 17.6; range: 13%–23%) was prominent in assemblage 2 with no trending change. The araphid/raphid benthic decline was signaled by *Staurosira venter* which continued with a decline from assemblage 1 registering a final abundance at 2210 cal BP of <3%. *Pinnularia* spp. declined from assemblage 1 and was consistently between 1% and 3%. In contrast, *Sellaphora* spp. (13%), *B. neoexilis* (12%), and *Encyonopsis microcephala* (10%) each showed increases through this interval (Figure 3). The planktic taxa remained low during this period (abundance <2.5%) with a planktic:benthic ratio of <0.03.

Assemblage 3: Raphid benthic stabilization (100–63 cm; ca. 2210–1270 cal BP; n = *38)*

This benthic littoral signal was characterized by decreased abundances of *Achnanthidium* spp. (5%–16%) and the disappearance of *S. venter* (Figure 3). *Navicula* spp. (median: 21%; range: 15%–29%) was the most consistent and trendless, while *Nitzschia* spp. (primarily *N. alpina*) increased into more recent times (median: 26.9; range: 18%–40%). Other taxa that became prominent throughout this period included *S. pupula* (3%–9.5%), and *B. neoexilis* (4%–14%). *Pinnularia biceps* was consistently present, while *Stauroneis* spp. (primarily *S. gracilis* and *S. amphicephala*) gradually declined into the next assemblage (*Pinnularia* and *Stauroneis*: <1%–12%). The planktic *L. intermedia* showed a consistent abundance through this period (<8%) with *Cyclotella* spp., and *D. pseudostelligera* present in low numbers (<3%). The planktic:benthic ratio was <0.02.

Assemblage 4: Benthic/planktic transition community (62–48 cm; ca. 1270–980 cal BP; n = *15)*

This assemblage was characterized by changes in specific taxa abundances (Figure 3). *Cyclotella* spp. dominated the planktic taxa (<12%) in the later part of this period. In contrast, *D. pseudostelligera* (<11%) and *L. intermedia* (<11%) had abundance peaks mid-way through this period and then declined. The planktic:benthic ratio was <0.1. *Encyonopsis* spp. (specifically *E. microcephala*, 4%–15%) also increased then decreased throughout this period. There were also increases in the relative abundances of *B. neoexilis* (<19%) and *Achnanthidium* spp. (7%–16%). *Nitzschia* spp. maintained high abundances (median: 23%; range 20%–30%), similar to the early levels of Assemblage 3. *Navicula* spp. (median: 18%; range: 15%–23%) also continued to be a major component of the diatom community. Finally, *Cyclotella* spp., *Sellaphora* spp., *Stauroneis* spp., *Pinnularia* spp., and *Neidium* spp. increased after the WRAe but were declining by 980 cal BP.

Assemblage 5: Planktic/benthic community (47–40 cm; ca. 980–800 cal BP; n = *8)*

This planktic/benthic community was characterized by an increase in *L. intermedia* (range: 5%–11%) and *D. pseudostelligera* (<5%) with a decline in and then subtle increase in *Cyclotella* spp. (<6%) (Figure 3). The planktic:benthic ratio was <0.14. There were also elevated abundances of the benthic *B. neoexilis* (median: 15%; range: 11%–17%) and *Navicula* spp. (median: 22%; range: 18%–30%). *Nitzschia alpina* declined in this zone relative to the previous assemblage. Compared to Assemblage 4, there were also reductions in *Achnanthidium* spp., *Encyonema* spp., and *S. pupula. Pinnularia biceps* and *Stauroneis* spp. had peak levels at the early beginning of this period, but declined to minimal numbers (almost disappeared from the record in the more recent sediments).

Assemblage 6: Planktic/benthic stabilization (39–13 cm; ca. 800–200 cal BP; n = *26)*

The assemblage in this period was stabilized with a planktic/benthic community dominated by *L. intermedia* (median: 9; range: 1%–21%), *B. neoexilis* (median; 16; range: 11%–20%), and *Navicula* spp. (median: 22%; range: 16%–30%) (Figure 3). The planktic:benthic ratio was highest in this assemblage at <0.3. Through this interval, *B. neoexilis* had consistent numbers, while *D. pseudostelligera* and *Cyclotella* spp. fluctuated with higher abundances in the most recent sediments (200 cal BP). *Navicula* spp. declined to abundances similar to Assemblage 1 (median: 16; range: 10%–21%). *Encyonopsis* spp. (5%–12%) was also an important component of the assemblage although this taxon declined in the uppermost sediments. In the most recent sediments *Neidium* spp. became more prominent in the assemblage. *Achnanthidium* spp., *P. biceps*, *E. silesiacum/minutum*, *Cymbopleura* spp., and *S. pupula* were at their lowest relative abundances in the upper most sediments in this study.

Intervals of assemblage change

The transition between assemblages 1 and 2 (460 BC, Iron Age Cold Epoch) was marked by an increase in SARs, EM4, and decline in EM3. Associated with these particulate changes there were declines in *Cyclotella* spp., *Pinnularia* spp., and *Staurosira venter*. The change from Assemblage 2 into Assemblage 3 (200 BC, Roman Warm Period) was characterized by the termination of the araphid benthic community, specifically by the disappearance of *S. venter. Sellaphora pupula* showed a peak abundance, with increases in the less abundant *Pinnularia* spp. and *Neidium* spp. and the start of a decline in *Encyonema* spp. with a brief decline in the grain sizes. The proportions of end members EM3 and EM4 were low. The transition to a benthic stable lake system from assemblage 3–4 was marked by a decline in TSI, limited S2 and subsequent short spikes in Cu, Zn and Pb. *Achnanthidium* spp, *Diploneis* spp., *B. neoexilis*, and *D. pseudostelligera* increased, while *Nitzschia* spp. and *S. pupula* declined. The transition into the MWA (Assemblage 4–5) was characterized by declines in *Achnanthidium*, *Nitzschia, Pinnularia*, *Stauroneis*, *Sellaphora*, and stabilization of the planktic taxa. EM4 was increasing during this interval change and EM2 was declining. The transition into the LIA (Assemblage 5–6) showed an enhanced planktic community, increases in *Neidium* spp. and *Diploneis* spp. along with a decline in *Achnanthidium, Encyonopsis*, and *Nitzschia*. There was also a spike of Cd during this transition.

Redundancy analysis (RDA)

RDA analysis revealed relationships between diatom assemblages, sedimentary particle size, and the concentration of elements (Figure 4). Particle size fractions were prominent along axis one, while Ca concentration was aligned between axis one and two. Collectively, the selected variables explained 28.8% of the variance in the diatom assemblages, with Fe, Ca, and EM1, EM2, and EM3 being important indicators of community change. Arsenic was not considered in this analysis due to anthropogenic contamination in the upper sediments and S2 was excluded due to poor quantitative resolution. TSI was not a significant factor in explaining assemblage changes, although it was aligned on axis one with grain size.

Discussion

The diatom composition of Pocket Lake over the last 2800 years has followed a predictable acidification trajectory of lake ontogeny (aging) observed in other Arctic and boreal regions, but not directly linked to climate (e.g. Engstrom et al., 2000; Fritz and Anderson, 2013; Laws et al., 2015). Earlier millennia show characteristic higher alkalinity and diatom growth conditions which through time change to less alkaline or acidic oligotrophic environments. Pocket Lake showed a decline in autochthonous productivity (S2), with trending increases in Ca, S, and Fe across assemblages. The early loss of an alkaline taxon *S. venter* and subsequent increase in circum-neutral to acidophilic-trending taxa like *Brachysira neoexilis*, *Neidium* spp., and *Diploneis* spp. further support lake aging processes. At present, the lake is small, shallow, and surrounded by exposed bedrock and a meadow. The terrestrial vegetation (Black spruce, willows, sedges, mosses, and grasses) are indicative of low productivity environments under circum-neutral to acidic conditions (current lake pH 7.7).

Superimposed on acidification trends driven by natural aging, Pocket Lake from ~2850 to 200 cal BP, further comprises six paleoecological diatom assemblages that are associated with cycles in climate change, precipitation (small changes in sediment loading from runoff), and local rock and sediment chemistry (Figure 3). Diatom community shifts for periods in the Iron Age Cold Epoch, Roman Warm Period, MWA, and the LIA are identified by moderate shifts in the assemblages. In addition, volcanic eruption events (one, possibly two) are associated with diatom species shifts in the lake. The sediment record also documents changes in particulate grain size distributions and metal inputs (Cu, Zn, Pb spikes) that could be driven by different relative amounts of rainfall and snowmelt, as well as changes in surface and subsurface pathways of runoff into the lake. Nutrients are not a prominent driver of total numbers and diversity in Pocket Lake. Phosphorus concentrations in the sediments (73–118 mg kg^{-1}), irrespective of mobility in the sediments, do not reflect significant nutrient enrichment for autochthonous primary production. Furthermore, a positive correlation with Ca (rho = 0.74, $p = 0.001$; $n = 118$), and weak negative correlation with Fe (rho = −0.20, $p = 0.1$; $n = 118$) suggest that sedimentary P is derived from more than one source. An anthropogenic impact of mining is also documented with the downward mobilization of As and Sb into the sediment record invading back through 900 years of paleo-sediment history. This small lake with an equally small catchment area was able to capture distinct changes in the environment from fine local impacts to regional and global changes in climate, although not enough to identify higher frequency global climatic oscillations.

Diatoms, climate, and hydroecological indicators

The most significant change observed in Pocket Lake from 2000 to 2800 years ago was the decline of *S. venter* through Assemblage 1 and its ultimate disappearance by the end of Assemblage 2 (ca. 2020 cal BP). Increases in SAR, and EM4 coupled with the changing diatom composition align with a documented cold spell during the Iron Age Cold Epoch (Swindles et al., 2007). In these early assemblages, diatom populations changed characterized by lower planktic and naviculoid numbers and increases in *Nitzschia* and *Achnanthidium* spp. Increased surface runoff as indicated by higher proportions of the coarser grained EM4, identified in RDA analysis, coupled with the changing diatom composition suggests more unsettled, possibly turbid water conditions in the benthic littoral regions of the lake. This hypothesis fits well with development of an extended cold wetter period during the Iron Age Cold Epoch, characterized by more surface water inflow. Although there has been taxonomic confusion related to the identification of *S. venter* (in many publications generally listed as *Fragilaria venter* Ehrenberg), the morphology conforms with descriptions of specimens within this species complex from previous circumpolar Arctic studies (e.g. Paull et al., 2008). *Staurosira venter* is generally associated with alkaline, variable and unpredictable oligotrophic limnological conditions, which is typical for tundra lakes in post-glacial settings (Bouchard et al., 2004; Laing et al., 1999; LeBlanc et al., 2004). Lotter and Bigler (2000) suggested that *S. venter* is an r-strategist that colonizes new aquatic systems quickly, where unstable, rapidly shifting environments are common. For example, peaks in the relative abundance of *S. venter* often coincide with early lake development where changing water levels create inconsistent environments for littoral colonization (Schmidt et al., 2004). In the Arctic numerous studies have reported *S. venter* as common in Holocene fossil samples but rarer to absent in modern samples (e.g. Antoniades et al., 2008; Rühland and Smol, 2005) supporting a widespread impact of climate on northern aquatic systems.

The ultimate disappearance of *S. venter* is aligned with the start of Roman Warm Period (200 BC [2210 cal BP]) (Bianchi and McCave, 1999). Through this warmer period (Assemblage 3) SARs are lower, there was a shift to stable levels of smaller particulates (EM2 and EM4) and consistent lake productivity indicated by S2 (Rock eval) and TSI levels. Through this period there is a diverse distribution of diatom taxa indicating stable conditions across lake habitats. Closer to the transition between Assemblages 3 and 4, a return to higher numbers of *Nitzschia* spp. is observed with declines in the planktic *Cyclotella distinguenda*

and lower numbers of naviculoids, suggesting a return to a more unpredictable and varied lake system. The relative abundances of EM2 and EM3 were consistent through the period of Assemblage 3 suggesting stable surface water inputs to Pocket Lake, while periodic increases in Cu, Zn, and Pb suggest sporadic changes in subsurface water loading (see *chemical drivers* below).

A period of low TSI (lowest during the study interval) and minimal S2 productivity marked the assemblage change from Assemblage 3 to Assemblage 4 (750 AD, 1260 cal BP). Globally, this was a short cold cycle within the Dark Ages Cold Period, which has a possible link to the Rabaul Eruption from Papau New Guinea, or an Icelandic eruption (Gibbons, 2018; Larsen et al., 2008; PAGES2K Consortium, 2017). Immediately after this transition in Pocket Lake TSI and S2 levels recovered, particulate composition did not change and spikes of Cu, Zn, and Pb were recorded. The transition from Assemblage 3 to Assemblage 4 was a short cold period followed by sporadic periods of subsurface inflow (see *chemical drivers* below). The benthic *Diploneis* spp. and planktic *L. intermedia*/*D. pseudostelligera* appeared in numbers, with increases in *Achnanthidium* spp., and *B. neoexilis*, while *Nitzschia* spp. declined. Assemblage 4 in Pocket Lake represents biomass increases across lentic and lotic habitats with a possible change in lake pH. *Brachysira neoexilis* is a benthic dweller with an established autecology for oligotrophic slightly alkaline to circum-neutral to slightly acidic conditions (Siver et al., 2011, Van de Vivjer et al., in press).

Assemblage 5 covers a short period (960–800 cal BP) recognized as part of the Medieval Warm Anomaly (Mann et al., 2009). Sedimentation and TSI were consistent through the MWA assemblage interval with a decline in EM4, increase in EM3 and consistent EM2 levels. The decline in relative abundance for *Nitzschia* spp. with consistent abundances of *B. neoexilis*, *Achnanthidium* spp., *L. intermedia*, *D. pseudostelligera*, and *Cyclotella* spp. suggest stable environmental conditions (no dramatic fluctuations in surface and ground water inputs). However, the decline or absence of *Pinnularia*, *Sellaphora*, and *Stauroneis* taxa indicates a less biologically diverse system compared to the Roman Warm Period. The appearance of Cd at the beginning and end of Assemblage 5 is consistent with preindustrial levels (Håkanson, 1980). Although we cannot identify a causal explanation for these Cd peaks, it is recognized that Cd becomes mobile under more acidic conditions (Fjeld et al., 1994) and these are aligned with minor increases of *B. neoexilis*, (Figure 3). In this study the MWA was not notably more productive relative to the other assemblages as indicated by Rock-Eval S2 data and planktic diatom relative abundances. Jomelli et al. (2016) have similarly noted regional cooling in the western Arctic during the MWA and tentatively attribute this to volcanic and /or atmospheric circulation anomalies related to solar forcing. During these cold periods there could have been changes in relative amounts of snowmelt versus rainfall-generated runoff from the catchment that enhanced indirect effects that ultimately led to reduced productivity (Figure 4).

The Little Ice Age is identified by Assemblage 6, which is characterized by a substantive increase in plankton (*D. pseudostelligera*, *L. intermedia*), stable abundance of *B. neoexilis* and declines in *Achnanthidium* spp., *Encyonopsis* spp., *Nitzschia* spp., and *Navicula* spp. Combined with consistent EM2 levels and two spikes of EM1 particulates, Pocket Lake has more lotic activity with a productive but less diverse benthic littoral region. Early in this LIA period, elevated levels of Pb, Zn, and Cd are aligned with *L. intermedia* peaks and suggest an early wet period with subsurface water inputs to the lake. Although an enrichment of small planktic genera like *Cyclotella*, *Pantoscekiella*, *Discotella*, and *Lindavia* is considered indicative of warmer temperatures (Saros and Anderson, 2015), increases in the relative abundance of these genera during cool periods, such as during the LIA in Pocket Lake, has also been observed in many chemically dilute lakes at high altitudes and northern-latitudes (Gregory-Eaves et al., 1999; Karst-Riddoch et al., 2005; Kling and Håkansson, 1988; Rühland and Smol, 2005). *Lindavia intermedia* and *D. pseudostelligera* are indicators of lower temperature and circum-neutral to moderately acidic surface water conditions, which can be found in limnological systems with variable runoff, as long as turbidity does not increase (e.g. Kipp et al., 2020). Thienpont et al. (2016) investigated the Pocket Lake diatom response to 20th century mining activity at the adjacent Giant Mine and found that *D. pseudostelligera* disappeared from the lake and more acidophilic taxa within the genus *Navicula* (e.g. *N. cryptocephala sensu lato*) increased coincident with increasing concentrations of mining derived As deposition into the lake. At one point $>30{,}000\,mg\,kg^{-1}$ of As in the uppermost sediments of Pocket Lake was measured (Thienpont et al., 2016). However, as noted in their research the increase in As was also associated with an influx of other mine-derived metals and metal(loid) contaminants, including Pb, Hg, Fe, Mn, and Sb. Therefore, it is not clear in the present history of Pocket Lake, whether As alone is exerting a toxic effect over the abundance of diatoms, specifically *D. pseudostelligera.*

The observed WRAe deposit (<5 mm), derived from the Plinian-style Mount Churchill Eruption (White River Ash, ~1100 cal BP; Patterson et al., 2017) had a short-term impact on sediment size fractionation, and metals but resulted in no immediate change in the diatom community (Hutchinson et al., 2019). However, after the event there were increases in *Stauroneis* spp., *Sellaphora* spp., *Pinnularia* spp., *Neidium* spp., and *Encyonopsis* spp. which declined into the transition Assemblage 4–5. Minor changes in pH and alkalinity likely caused the observed increases in these naviculoid diatoms.

Sediment drivers

Transport of solutes and sediments in the Pocket Lake catchment is predominately driven by the spring freshet. Summer rainfall events typically do not overcome the summer storage capacity in catchment soils nor do they have adequate intensity to generate significant transport of sediment into a lake basin (Spence and Woo, 2003; Cockburn and Lamoureux, 2008a, 2008b). Fluctuations in SARs over the last 2800 years and differences observed based on particle size analysis indicate both autochthonous and allochthonous influences are recorded in the sediments of Pocket Lake. The distributions of EM2 and EM3 were characterized by similarly comparable trends and were the dominant size classes in Pocket Lake. The period from 2600 to 2000 cal BP had a predominant EM3 and EM4 composition and higher SAR indicating a period of enhanced surface runoff which was followed by a period dominated by EM2 (2000–1100 cal BP), with little variation in the partitioning of end members, suggesting a period of relatively stable and consistent runoff and deposition. The disappearance of *S. venter* (ca. 2200 cal BP) an r-strategist, also supports the observation that a period of stability persisted in the lake during this time. The reduction of EM2 and EM3 at 55–56 cm is the result of the White River Ash tephra deposit 1100 years ago cal BP (Hutchinson et al., 2019; Patterson et al., 2017). After the eruption and deposition of tephra, there is a shift in grain size to EM4 during the MWA (53–40 cm; ca. 1100–800 cal BP). The larger grain size sediments and slightly higher SAR indicate enhanced runoff from the catchment, possibly due to more snow/rain events and/or less stable terrestrial conditions (soil buffering capacity) after cessation of the WRAe tephra impact on the region. Concomitant structural changes in the Pocket Lake aquatic community composition are characterized by a decline in benthic *Achnanthidium* and *Nitzschia* densities and an increase in *B. neoexilis*, a species which is typically found under relatively stable and circumneutral to mildly acidic water conditions. With the exception of two short periods (700 and 200 cal BP) of EM4 deposition, EM2 dominated the LIA, showing a consistent pattern of terrestrial runoff into the lake during the LIA.

Chemical drivers

Patterns in the distribution of metals in the sedimentary record of Pocket Lake indicate linkages with terrestrial runoff and lake sediment chemistry. The abundant elements, Fe, Ca, and S fluctuated slightly at certain periods in the sedimentary record (e.g. reduction during the White River Volcanic event (Figure 3, 55–56 cm)), but were otherwise consistent throughout the examined ~2800 year period. Fe showed the strongest RDA signal with declining concentrations from 2800 cal BP associated with decreasing particle size (Figure 4). Average S concentrations increased from bottom to top of the core supporting the interpretation of progressive acidification towards a neural pH for Pocket lake through 2800 years. Moderate Ca concentrations also increased further suggesting higher soluble levels of Ca in the waters of Pocket Lake with lower pH trending towards circumneutral levels. The less abundant metals (e.g. Cu, Zn, Pb, Cd) exhibited periodic increases with implications for allochthonous loading from soils (McLean and Bledsoe, 1992). In the small catchment of Pocket Lake, dominated by exposed bedrock, the primary source for Cu, Zn, and Pb is the soil-filled valley on the north side of the lake and associated dyke drainage. Iron and Mn-oxyhydroxides in soils have a strong affinity for trace metals, including Cu, Pb, and Zn (Bauer and Blodau, 2006; Benjamin and Leckie, 1981a, 1981b; Bowell, 1994). The dissolution and/or desorption of Cu, Pb, and Zn from Fe, Mn-oxyhydroxides in soils during snowmelt could lead to substantial export of these metals from the catchment to the lake. Small trenches exposing Cu, Pb, and Zn mineralization associated with the margin of the primary dyke illustrate at least one direct pathway for allochthonous organics and mineral input. Consequently, large differences in snowpack may lead to variations in transport of these trace metals to the lake. The poor correlation of Pb with particle size sediment deposition suggest that the base metals were transported in the dissolved soil fraction, consistent with snowmelt passing through surface organic soils without significant erosion. The 10 evident spikes of Cu, Zn, Pb in Pocket Lake over 2800 years could represent periods of deeper snow pack and enhanced snowmelt subsurface runoff. Two larger runoff periods were present in the LIA (Assemblage 5), none during the MWA (Assemblage 4), one during the benthic/planktic mixed community period (Assemblage 3), four during the raphid benthic signal (Assemblage 2) and three within the raphid/araphid benthic period (Assemblage 1).

Irrespective of the mechanism driving variation in the chemical stratigraphy of sediments in Pocket Lake, it is clear that the water chemistry changed and was associated with changes in the limnology of the lake. The Cu, Pb, Zn peaks were associated with the diatoms *B. neoexilis* and *L. intermedia*. These taxa are indicative of pH and alkalinity changes in lakes (e.g. Siver et al., 2011). In addition, there were two increases in Cd during the MWA (Assemblage 4), not linked to grain size, but associated with small increases in diatoms *Stauroneis*, *Sellaphora*, and *Pinnularia*. It is not clear why Cd increases were independent of other metals, but it is possible that increased productivity (indicated by an increasing planktic community) during the MWA, created more organic ligands and increasing Cd mobility during significant runoff events (Benjamin and Leckie 1981a, 1981b). Lake level changes through the last 2800 years could also alter lake sediment chemistry. However the steady SARs (0.3–0.6 mm $year^{-1}$) over long intervals did not correlate with metal changes in the sediment, nor with changes in the plankton. Indeed, the period with the lowest SAR (200–800 cal BP) had the largest planktic signal.

Anthropogenic impacts

One of the clearest geochemical patterns in the sedimentary record from Pocket Lake was the continuous decline of As and Sb concentrations from the uppermost sediments (200 cal BP) to approximately 55 cm (ca. 1100 cal BP). Extremely high concentrations of sedimentary As (>30,000 mg kg^{-1}) and Sb (up to 1500 mg kg^{-1}) were measured in the near-surface sediments of Pocket Lake in a separate study and were associated with the gold mine roaster smelting derived atmospheric deposition of As and Sb in the region (Thienpont et al., 2016). Arsenic and Sb are highly mobile under reducing conditions, such as those present in organic-rich sediments, and the upward and downward mobility of these elements has been described previously in the literature and the region (Dixit and Hering, 2003; Schuh et al., 2018). The long core collected from this study (>1 m) shows that downward mobility of As and Sb, and subsequent reprecipitation of As and Sb minerals can be an important confounding variable deeper in the sediments than previously expected. This is particularly the case where large concentration gradients in sediment porewaters, generated from the dissolution of high concentrations of solid phase As, would support high diffusive fluxes of these elements. This has important implications for the use of short cores (<30 cm) for estimating pre-mining background conditions of redox sensitive elements, such as As and Sb. In addition, Cheney et al. (2020) recently proposed that background levels of sedimentary As in many lakes from the Yellowknife region may be elevated relative to others regions in Canada and the world due to solubility and geogenic sources of As in the region. The data from this study highlight the importance of considering the downward mobilization of metals(oids) like As in lake sediments. In Pocket Lake, there has been a downward mobilization of As into sediments that date from well before the onset of anthropogenic mining activities (>1000 years BP). However, slight increases in the concentration of As and Sb is sediments from the bottom of the core also suggest that at the end of the Holocene Thermal Maximum, increased chemical and physical weathering associated with warmer air temperatures may have resulted in increased geogenic loading and/or sequestration, possibly mediated by organic matter (Galloway et al., 2018).

Summary

This study identified clear changes in living conditions and metal contamination levels from a Precambrian Shield aquatic system that can be linked to changes in solar radiation output, regardless of natural lake aging trends and recent mining contamination. Pocket Lake, a small shallow lake with limited terrestrial production demonstrates an ontogeny trajectory similar to that observed in other Arctic lakes for an interval spanning the last 2800 cal BP. In addition, Pocket Lake displays evidence of clear episodic shifts in climate documented by diatom assemblages, which is well aligned with projected climate cycles across the circumpolar Arctic (ACIA, 2004; MacDonald, et al., 2008). Diatom community shifts (assemblages) for periods in the Iron Age Cold Epoch, Roman Warm Anomaly, MWA and the LIA were linked to climatic conditions characterizing these intervals. Two volcanic events are also associated with diatom species shifts in the lake. However, there is no evidence that the finer Pacific Decadal Oscillation influenced the chemistry and biology of Pocket Lake. Productivity (S2), grain size, SAR, and elemental metals influenced the makeup of the six CONISS determined diatom assemblages. TSI appears to have played a role in the changing diatom community and associated productivity (S2), but was not significantly identified. Nutrients (e.g. P) did not play a significant role. Pocket Lake showed brief periods of metal loading (Cu, Zn, Pb) over the 2800 years of study producing short-term effects, but no permanent effect on diatom community assemblages. The As contamination of sediments deposited during the last ca. 900 years of lake history was the result of post depositional remobilization, and had no impact on the paleo-community assemblage/ environmental relationships recorded in Pocket Lake for this interval. The small lake with an equally small catchment area was able to capture distinct changes in the

environment from fine local impacts to regional and global changes in climate. This study attained the goal of documenting subtle assemblage changes in the lake ecology of Pocket Lake prior to mining contamination, which highlights the utility of using long paleolimnological records for assessing lake susceptibility pre and ultimately post conditions of anthropogenic stress.

Acknowledgements

We would especially like to thank and acknowledge the excellent, extensive, and probing reviews by Dr. H. Elizabeth Anderson, two independent reviewers, one internal reviewer, and the associate editor for this manuscript.

Funding

The author(s) disclosed receipt of the following financial support for the research, authorship, and/or publication of this article: This research was funded by a Cumulative Impact and Monitoring Program Grant, (#00140) to CS with in-kind contributions from the Northwest Territories Geological Survey (HF), the Geological Survey of Canada (Arcticnet P51, NRCan 20200634; JMG), and the North Slave Métis Alliance. Research analysis funding was through a RAC 2018-2020 grant (PBH) from the Canadian Museum of Nature. Additional financial support was provided by Natural Resources Canada (NRCan) via a Research Affiliate Program (RAP) bursary awarded to SJH and NN, a NRCan Clean Technology Grant (#CGP-17-0704) to RTP, (Environmental Geoscience Program activity via JMG), and a NSERC Discovery Grant (RGPIN 2018-05329) to RTP. JMGs contributions to this work was conducted under the AIAS-COFUND II fellowship programe that is supported by the Marie Skłodowska-Curie actions under the European Union's Horizon 2020 (grant agreement no. 754513), the Aarhus University Research Foundation, and a POLAR Knowledge Canada Grant to JMG and RTP (Grant Number #1516-149).

ORCID iD

Paul B Hamilton https://orcid.org/0000-0001-6938-6341

Supplemental material

Supplemental material for this article is available online.

References

ACIA (2004) *Impacts of a Warming Arctic: Arctic Climate Impact Assessment*. Cambridge: Cambridge University Press, p. 1042.

Antoniades D, Hamilton PB, Douglas MSV et al. (2008) Diatoms of North America: The freshwater–floras of Prince Patrick, Ellef Ringnes and northern Ellesmere Islands from the Canadian Arctic Archipelago. *Iconographia Diatomologica* 17: 1–649.

Bahls L, Boynton B and Johnson B (2018) Atlas of diatoms (Bacilariophyta) from diverse habitats in remote regions of western Canada. *Phytokeys* 105: 1–186.

Bauer M and Blodau C (2006) Mobilization of arsenic by dissolved organic matter from iron oxides, soils and sediments. *Science of the Total Environment* 354: 179–190.

Benjamin MM and Leckie JO (1981a) Multiple-site adsorption of Cd, Cu, Zn, and Pb on amorphous iron oxyhydroxide. *Journal of Colloid and Interface Science* 79: 209–221.

Benjamin MM and Leckie JO (1981b) Conceptual model for metal-ligand-surface interactions during adsorption. *Environmental Science and Technology* 15(9): 1050–1057.

Bennike O, Brodersen KP, Jeppesen E et al. (2004) Aquatic invertebrates and high latitude paleolimnology. In: Pienitz R, Douglas MSV and Smol JP (eds) *Long-Term Environmental Change in Arctic and Antarctic Lakes*. Dordrecht: Springer, pp.159–186.

Bianchi G and McCave I (1999) Holocene periodicity in North Atlantic climate and deep-ocean flow south of Iceland. *Nature* 397: 515–517.

Blaauw M and Christen JA (2011) Flexible paleoclimate age-depth models using an autoregressive gamma process. *Bayesian Analysis* 6: 457–474.

Blaauw M and Christen JA (2013) Bacon manual. Available at: http://chrono.qub.ac.uk/blaauw/manualBacon_2.2.pdf (accessed 5 April 2021).

Blott SJ and Pye K (2001) GRADISTAT: A grain size distribution and statistics package for the analysis of unconsolidated sediments. *Earth Surface Processes and Landforms* 26: 1237–1248.

Bouchard G, Gajewski K and Hamilton PB (2004) Freshwater diatom biogeography in the Canadian Arctic Archipelago. *Journal of Biogeography* 31(12): 1955–1973.

Bowell RJ (1994) Sorption of arsenic by iron-oxides and oxyhydroxides in soils. *Applied Geochemistry* 9: 279–286.

Boyle RW (1960) *The Geology, Geochemistry and Origin of Gold Deposits of the Yellowknife District. Geological Survey of Canada Memoir 310*. Ottawa, Ontario: Department of Mines and Technical Surveys Canada, p. 193.

Brown IC (1955) Late faults in the Yellowknife area. In: *Geological Association of Canada. Proceedings*, Toronto, Ontario, 1955, vol. 7, pp.128–138.

Bronk Ramsey C (2009) Bayesian analysis of radiocarbon dates. *Radiocarbon* 51: 337–360.

Callaghan TV, Jonasson C, Thierfelder T et al. (2013) Ecosystem change and stability over multiple decades in the Swedish subarctic: Complex processes and multiple drivers. *Philosophical Transactions of the Royal Society B: Biological Sciences* 368(1624): 20120488–20120488.

Carrie J, Sanei H and Stern GA (2012) Standardization of rock-eval pyrolysis for the analysis of recent sediments and soils. *Organic Geochemistry* 46: 38–53.

Cheney CL, Eccles KM, Kimpe LE et al. (2020) Determining the effects of past gold mining using a sediment palaeotoxicity model. *Science of the Total Environment* 718: 137308.

Cockburn JMH and Lamoureux SF (2008a) Hydroclimate controls over seasonal sediment yield in two adjacent High Arctic watersheds. *Hydrological Processes* 22(12): 2013–2027.

Cockburn JMH and Lamoureux SF (2008b) Inflow and lake controls on short-term mass accumulation and sedimentary particle size in a High Arctic lake: Implications for interpreting varved lacustrine sedimentary records. *Journal of Paleolimnology* 40(3): 923–942.

Crann CA, Patterson RT, Macumber AL et al. (2015) Sediment accumulation rates in subarctic lakes: Insights from 22 dated lake records and applications with age-depth modeling. *Quaternary Geochronology* 27: 131–144.

Dalton AS, Patterson TR, Roe HM et al. (2018) Late-Holocene climatic variability in Subarctic Canada: Insights from a high-resolution lake record from the central Northwest Territories. *PLoS One* 13(6): 1–21.

Delworth TL, Zeng F, Vecchi GA et al. (2016) The North Atlantic Oscillation as a driver of rapid climate change in the Northern Hemisphere. *Nature Geoscience* 9(7): 509–512.

Dietze E, Maussion F, Ahlborn M et al. (2014) Sediment transport processes across the Tibetan Plateau inferred from robust grain-size end members in lake sediments. *Climate of the Past* 10(1): 91–106.

Dietze E, Hartmann K, Diekmann B et al. (2012) An end-member algorithm for deciphering modern detrital processes from lake sediments of Lake Donggi Cona, NE Tibetan Plateau, China. *Sedimentary Geology* 243–244: 169–180.

Dietze M and Dietze E (2016) *EMMAgeo: End-Member Modelling of Grain-Size Data*. R package version 0.94. Available at: https://CRAN.R-project.org/package=EMMAgeo (accessed 5 April 2021).

Dixit S and Hering JG (2003) Comparison of arsenic(V) and arsenic(III) sorption onto iron oxide minerals: Implications

for arsenic mobility. *Environmental Science and Technology* 37: 4182–4189.

Engstrom DR, Fritz SC, Almendinger JE et al. (2000) Chemical and biological trends during lake evolution in recently deglaciated terrain. *Nature* 408: 161–166.

Fjeld E, Rognerud S and Steinnes E (1994) Influence of environmental factors on heavy metal concentration in lake sediments in southern Norway indicated by path analysis. *Canadian Journal of Fisheries and Aquatic Sciences* 51: 1708–1720.

Fishbein E and Patterson RT (1993) "Error weighted maximum likelihood (EWML)" a new statistically valid method to cluster quantitative micropaleontological data. *Journal of Paleontology* 67: 475–486.

Fritz SC and Anderson NJ (2013) The relative influences of climate and catchment processes on Holocene lake development in glaciated regions. *Journal of Paleolimnology* 49: 349–362.

Galloway JM, Swindles GT, Jamieson HE et al. (2018) Organic matter control on the distribution of arsenic in lake sediments impacted by ~ 65 years of gold ore processing in subarctic Canada. *Science of the Total Environment* 622–623: 1668–1679.

Gajewski K, Hamilton PB and McNeely R (1997) A high-resolution proxy-climate record from an arctic lake with annually-laminated sediments on Devon Island, Nunavut, Canada. *Journal of Paleolimnology* 17(2): 215–225.

Gibbons A (2018) *Why 536 was 'the worst year to be alive'*. Science | AAAS. 15 November.

Gregory BRBG, Patterson RT, Galloway JM et al. (2021) The impact of cyclical, multi-decadal to centennial climate variability on arsenic sequestration in lacustrine sediments. *Palaeogeography, Palaeoclimatology, Palaeoecology* 565: 110189.

Gregory-Eaves I, Smol JP, Finney BP et al. (1999) Diatom-based transfer functions for inferring past climatic and environmental changes in Alaska, U.S.A. *Arctic Antarctic and Alpine Research* 31: 353–365.

Grimm EC (1987) CONISS: A FORTRAN 77 program for stratigraphically constrained cluster analysis by the method of incremental sum of squares. *Computers & Geosciences* 13(1): 13–35.

Guiry MD and Guiry GM (2020) *AlgaeBase. World-Wide Electronic Publication*. Galway: National University of Ireland. Available at: http://www.algaebase.org (accessed 13 April 2020).

Håkanson L (1980) An ecological risk index for aquatic pollution control. A sedimentological approach. *Water Research* 14: 975–1001.

Hamilton PB, Lavoie I, Alpay S et al. (2015) Using diatom assemblages and sulfur in sediments to uncover the effects of historical mining on Lake Arnoux (Quebec, Canada): a retrospective of economic benefits vs. environmental debt. *Frontiers in Ecology and Evolution* 3: 99.

Henderson JB (1985) Geology of the Yellowknife-Hearne Lake area, District of Mackenzie: A segment across an Archean basin. *Geological Survey of Canada, Memoir* 414: 135.

Hutchinson SJ, Hamilton PB, Patterson RT et al. (2019) Diatom ecological response to deposition of the 833-850 CE White River Ash (east Lobe) ashfall in a small subarctic Canadian lake. *PeerJ* 7: e6269.

Jamieson HE (2014) The legacy of arsenic contamination from mining and processing refractory gold ore at Giant Mine, Yellowknife, Northwest Territories, *Canada. Review in Mineralogy and Geochemistry* 79: 533–551.

Jomelli V, Lane T, Favie V et al. (2016) Paradoxical cold conditions during the medieval climate anomaly in the Western Arctic. *Scientific Reports* 6: 32984.

Karst-Riddoch TL, Pisaric MFJ and Smol JP (2005) Diatom responses to 20th century climate-related environmental changes in high-elevation mountain lakes of the northern Canadian Cordillera. *Journal of Paleolimnology* 33(3): 265–282.

Kipp RM, McCarthy M and Fusaro A (2020) *Discostella pseudostelligera* (Hustedt) Houk and Klee, 1939. Ann Arbor, MI: U.S. Geological Survey, Nonindigenous Aquatic Species Database, Gainesville, FL, and NOAA Great Lakes Aquatic Nonindigenous Species Information System. Available at: https://nas.er.usgs.gov/queries/GreatLakes/FactSheet.aspx?SpeciesID=1672 (accessed 5 April 2021).

Kling H and Håkansson H (1988) A light and electron microscope study of *Cyclotella* species (Bacillariophyceae) from central and northern Canadian lakes. *Diatom Research* 3: 55–82.

Krammer K and Lange-Bertalot H (1985–1991) Bacillariophyceae. In: Ettl H, Gerloff J, Heyinig H et al. (eds) *Süßwasserflora von Mittleuropa*. Stuttgart; New York, NY: Gustav Fischer Verlag.

Lafargue E, Marquis F and Pillot D (1998) Rock-eval 6 applications in hydrocarbon exploration, production and soil contamination studies. *Revue de l'Institut Français du Pétrole* 53(4): 421–437.

Laing TE, Ru KM and Smol JP (1999) Past environmental and climatic changes related to tree-line shifts inferred from fossil diatoms from a lake near the Lena River Delta, Siberia. *The Holocene* 5: 547–557.

Larsen LB, Vinther BM, Briffa KR et al. (2008) New ice core evidence for a volcanic cause of the A.D. 536 dust veil. *Geophysical Research Letters* 35(4): L04708.

Law AC, Anderson NJ and McGowan S (2015) Spatial and temporal variability of lake ontogeny in south-western Greenland. *Quaternary Science Reviews* 126: 1–16.

LeBlanc M, Gajewski K and Hamilton PB (2004) A diatom-based Holocene palaeoenvironmental record from a mid-arctic lake on Boothia Peninsula, Nunavut, Canada. The Holocene 14: 417–425.

Lotter AF and Bigler C (2000) Do diatoms in the Swiss Alps reflect the length of ice-cover? *Aquatic Sciences* 62(2): 125–141.

Macdonald RW, Harner T and Fyfe J (2005) Recent climate change in the Arctic and its impact on contaminant pathways and interpretation of temporal trend data. *Science of the Total Environment* 342(1–3): 5–86.

MacDonald GM, Kremenetski KV and Beilman DW (2008) Climate change and the northern Russian treeline zone. *Philosophical Transactions of the Royal Society B* 363: 2283e2299.

Macumber AL, Patterson RT, Galloway JM et al. (2018) Reconstruction of Holocene hydroclimatic variability in subarctic treeline lakes using lake sediment grain-size end-members. *The Holocene* 28(6): 845–857.

Macumber AL, Patterson RT, Neville LA et al. (2011) A sledge microtome for high resolution subsampling of freeze cores. *Journal of Paleolimnology* 45(2): 307–310.

Mann ME, Zhang Z, Rutherford S et al. (2009) Global signatures and dynamical origins of the Little Ice Age and Medieval Climate Anomaly. *Science* 326: 1256–1260.

McLean JE and Bledsoe BE (1992) *Behavior of metals in soils. EPA, Ground Water Issue. Technical Research Document Environmental Protection Agency EPA/540/S-92018*. Ada, OK: Environmental Research Laboratory, p. 25.

Miller GHJ, Brigham-Grette J, Alley RB et al. (2010) Temperature and precipitation history of the Arctic. *Quaternary Science Reviews* 29: 1679–1715.

Murray M (2002) Is laser particle size determination possible for carbonate-rich lake sediments? *Journal of Paleolimnology* 27: 173–183.

Nasser NA, Patterson RT, Roe HM et al. (2016) Lacustrine arcellinina (testate amoebae) as bioindicators of arsenic contamination. *Microbial Ecology* 72(1): 130–149.

Page 2k Consortium (2013) Continential-scale temperature variability during the past two millennia. *Nature Geoscience* 6: 339–346.

Paliy O and Shankar V (2016) Application of multivariate statistical techniques in microbial ecology. *Molecular Ecology* 25: 1032–1057.

Parsons M, LeBlanc KWG, Hall GEM et al. (2012) Environmental geochemistry of tailings, sediments and surface waters collected from 14 historic gold mining districts in Nova Scotia. *Geological Survey of Canada Open File* 7105: 326.

Patterson RT, Crann CA, Cutts JA et al. (2017) New occurrences of the White River Ash (east lobe) in Subarctic Canada and utility for estimating freshwater reservoir effect in lake sediment archives. *Palaeogeography, Palaeoclimatology, Palaeoecology* 477: 1–9.

Patterson RT and Kumar A (2002) A review of current testate rhizopod (thecamoebian) research in Canada. *Palaeogeography, Palaeoclimatology, Palaeoecology* 180(1–3): 225–251.

Paull TM, Hamilton PB, Gajewski K et al. (2008) Numerical analysis of small Arctic diatoms (Bacillariophyceae) representing the *Staurosira* and *Staurosirella* species complexes. *Phycologia* 47: 213–224.

Pienitz R, Smol JP and Macdonald GM (1999) Paleolimnological reconstruction of holocene climatic trends from two boreal treeline lakes, Northwest Territories, Canada. *Arctic, Antarctic, and Alpine Research* 31(1): 82–83.

Pisaric MFJ, St-Onge SM and Kokelj SV (2009) Tree-ring reconstruction of early-growing season precipitation from Yellowknife, Northwest Territories, Canada. *Arctic, Antarctic, and Alpine Research* 41(4): 486–496.

Reimer PJ, Bard E, Bayliss A et al. (2013) IntCal13 and Marine13 radiocarbon age calibration curves 0–50,000 years cal BP. *Radiocarbon* 55: 1869–1887.

Ritchie VJ, Ilgen AG, Mueller SH et al. (2013) Mobility and chemical fate of antimony and arsenic in historic mining environments of the Kantishna Hills district, Denali National Park and Preserve, Alaska. *Chemical Geology* 335: 172–188.

Rühland K and Smol JP (2005) Diatom shifts as evidence for recent Subarctic warming in a remote tundra lake, NWT, Canada. *Palaeogeography, Palaeoclimatology, Palaeoecology* 226(1–2): 1–16.

Sanei H and Goodarzi F (2006) Relationship between organic matter and mercury in recent lake sediment: The physical–geochemical aspects. *Applied Geochemistry* 21: 1900–1912.

Sanei H, Stasiuk LD and Goodarzi F (2005) Petrological changes occurring in organic matter from Recent lacustrine sediments during thermal alteration by Rock-Eval pyrolysis. *Organic Geochemistry* 36: 1190–1203.

Saros JE and Anderson NJ (2015) The ecology of the planktonic diatom *Cyclotella* and its implications for global environmental change studies. *Biological Reviews*, 90(2): 522–541.

Schmidt R, Kamenik C, Lange-Bertalot H et al. (2004) *Fragilaria* and *Staurosira* (Bacillariophyceae) from sediment surfaces of 40 lakes in the Austrian Alps in relation to environmental variables, and their potential for palaeoclimatology. *Journal of Limnology* 63: 171–89.

Siver PA and Hamilton PB (2011) Diatoms of North America: The freshwater flora of waterbodies on the Atlantic Coastal Plain. *Iconographia Diatomologica* 22: 1–916.

Schuh CE, Jamieson HE, Palmer MJ et al. (2018) Solid-phase speciation and post-depositional mobility of arsenic in lake sediments impacted by ore roasting at legacy gold mines in the Yellowknife area, Northwest Territories, Canada. Applied Geochemistry 91: 208–220.

Smol JP and Stoermer EF (2010) *The Diatoms: Applications for the Environmental and Earth Sciences*. Second edition. Cambridge: Cambridge University Press.

Spence C and Woo MK (2003) Hydrology of subarctic Canadian Shield: Soil-filled valleys. *Journal of Hydrology* 279: 151–166.

Steinhilber F, Beer J and Fröhlich C (2009) Total solar irradiance during the Holocene. *Geophysical Research Letters* 36(19): L19704.

Sulphur KC, Goldsmith SA, Galloway JM et al. (2016) Holocene fire regimes and treeline migration rates in sub-arctic Canada. *Global and Planetary Change* 145: 42–56.

Swindles GT, Plunkett G and Roe HM (2007) A delayed climatic response to solar forcing at 2800 cal. BP: Multiproxy evidence from three Irish peatlands. *The Holocene* 17(2): 177–182.

Thienpont JR, Korosi JB, Hargan KE et al. (2016) Multi-trophic level response to extreme metal contamination from gold mining in a subarctic lake. *Proceedings of the Royal Society B* 283: 20161125.

Upiter LM, Vermaire JC, Patterson RT et al. (2014) Middle to late-Holocene chironomid-inferred July temperatures for the central Northwest Territories, Canada. *Journal of Paleolimnology* 52(1–2): 11–26.

Van de Vijver B, Schuster TM, Kusber W-H et al. (2021). Revision of European Brachysira species (Brachysiraceae, Bacillariophyta): I. The Brachysira microcephala - B. neoexilis enigma. *Cryptogamie Algologie* (in press).

Van Hengstum PJ, Reinhardt EG, Boyce JI et al. (2007) Changing sedimentation patterns due to historical land-use change in Frenchman's Bay, Pickering, Canada: Evidence from high-resolution textural analysis. *Journal of Paleolimnology* 37(4): 603–618.

Viau AE and Gajewski K (2009) Reconstructing millennial-scale, regional paleoclimates of boreal Canada during the Holocene. *Journal of Climate* 2: 616–330.

Wolfe BB, Edwards TWD, Aravena R et al. (1996) Rapid Holocene hydrologic change along boreal treeline revealed by δ13 C and δ18 O in organic lake sediments, Northwest Territories, Canada. *Journal of Paleolimnology* 1996: 15: 171–181.